L. Duflot

Electron and pion response calorimeter weights and jet energy resolution

propaganda for CellNN and Eflow

~

What is responsible for jet low E response and resolution ?

1/ intrinsic calorimeter resolution

2/ cracks + dead material

3/ non linearity of response

3/ is the most important effect for low and medium energy jets

To improve on 2/ and 3/ you need to

* reconstruct individual E showers
* separate EM and HAD <u>particles</u> (not showers!)

then you can also apply CalWeights optimize for EM and HAD <u>particle</u> response and get the best of the CAL for 1/

DØ note 1300 (Bhat)

test beam e and π response

estimate of influence on jet response

DØ note 1502 (Borders)

optimization of CAL weight for single π

η and E dependant weights are best

$48\%/\sqrt{E} \longrightarrow 39\%/\sqrt{E}$

DØ note 2079 (Borders)

use Test Beam single particle response to simulate jet response

CAL weights optimization

here again η and E dependant weights are best

DØ note 1595 (Mieder + Astur)

jet response from single particle response

E scale estimates

Melissa Ridel

CellNN

* cell based cluster algorithm
* try to export the EM3 granularity to othe layers through energy sharing

our candidate algorithm for fine grained clustering in CAL

Melissa is trying now to derive a calibration of CellNN cluster

* single particle MC
* take the one the produce only one cluster
* EM crack corrections
  - based on distance to the crack
  - quite successful and probably enough for jets
* pion corrections much more tricky
  - need to separate pions in EM section from other
  - Crack corrections ?

→ taking only these single particle corrections brings back the jets to $R \simeq 0.98$

E flow

long term project

combine tracking information with CellNN

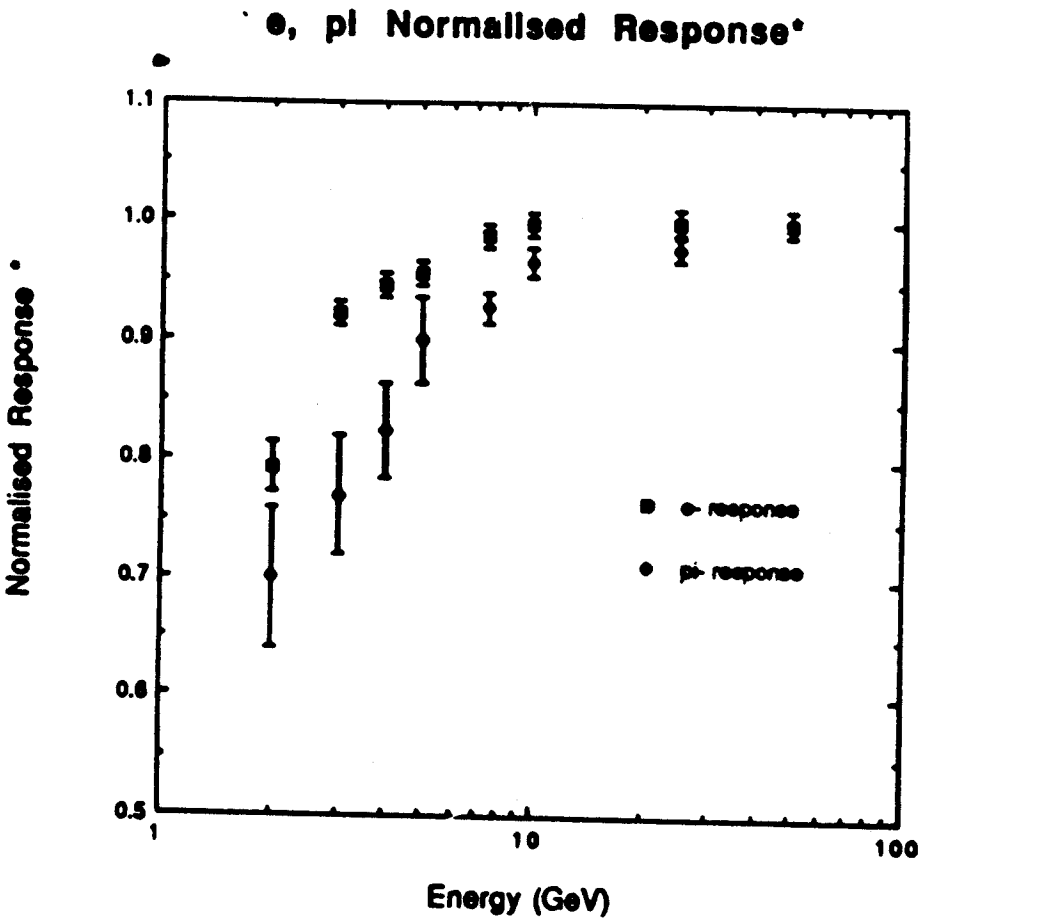

* Normalised to 50 GeV response

pi Normalised Response*

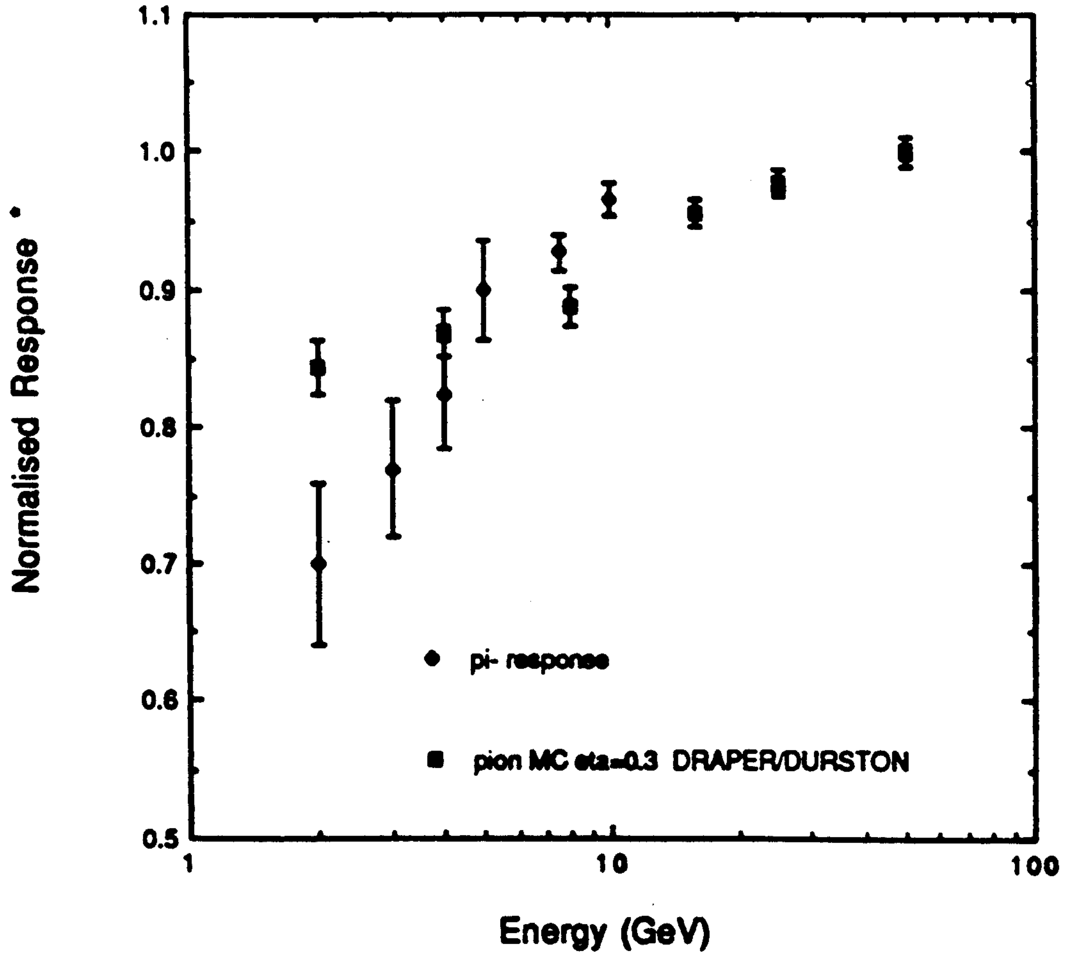

* Normalised to 50 GeV response

D/ 13n

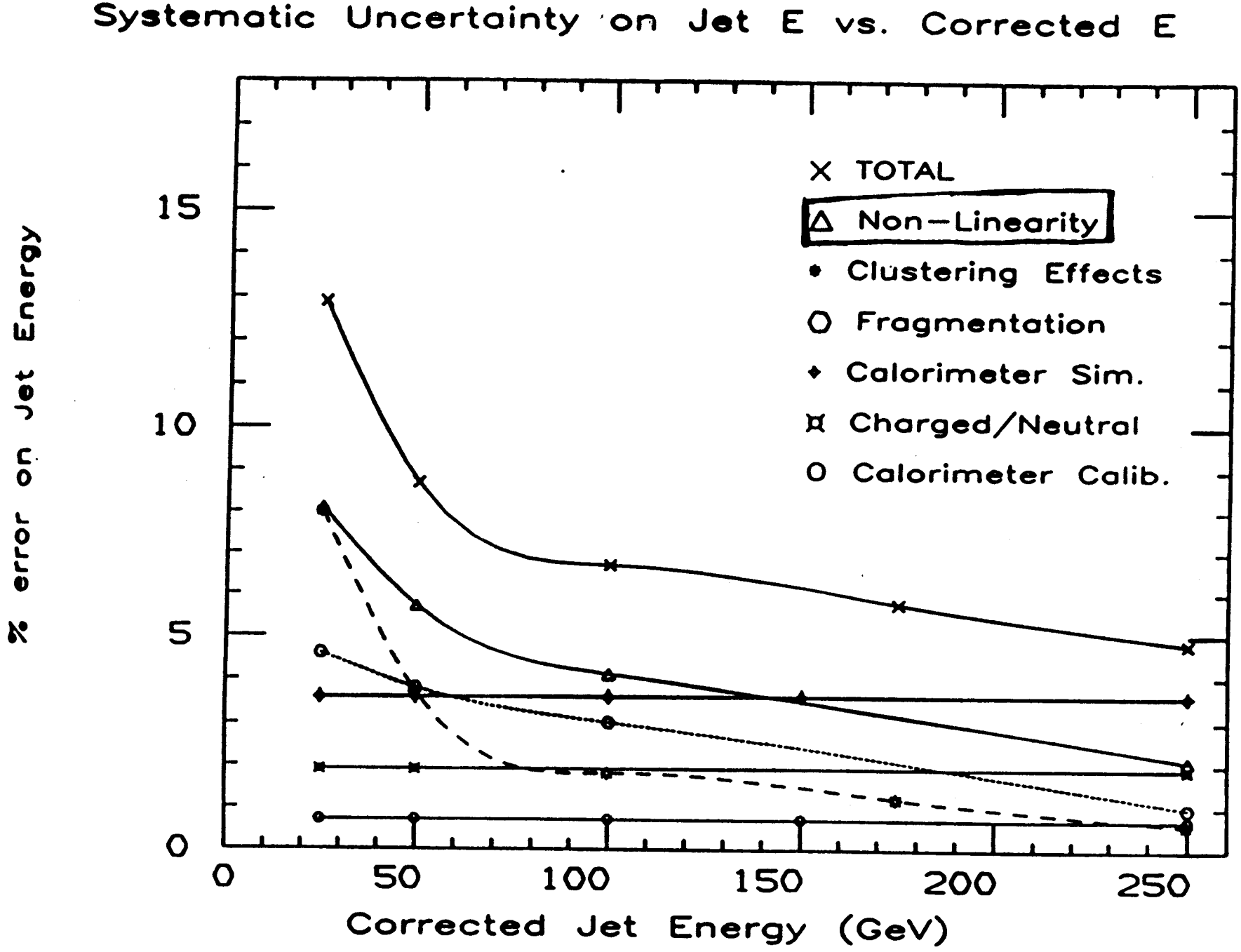

FIG. 11

DØ 1800

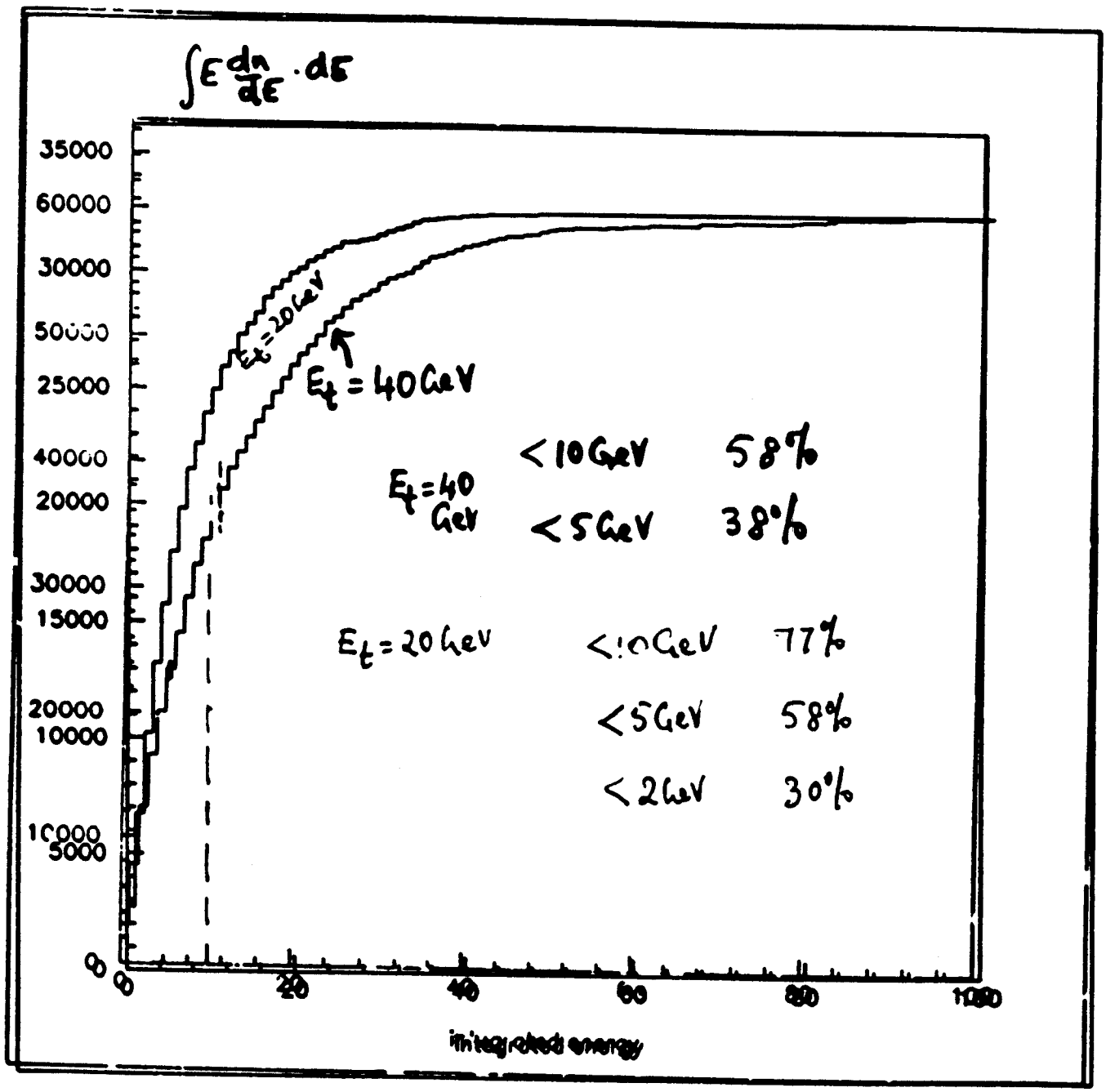
$\int E \frac{dn}{dE} \cdot dE$
35000
60000
30000
50000
25000
40000
20000
30000
15000
20000
10000
10000
5000
0
0
20
40
60
80
100
integrated energy
E_t=20GeV
E_t = 40GeV
E_t=40 GeV
<10GeV 58%
<5GeV 38%
E_t=20GeV
<10GeV 77%
<5GeV 58%
<2GeV 30%

Dϕ 1300

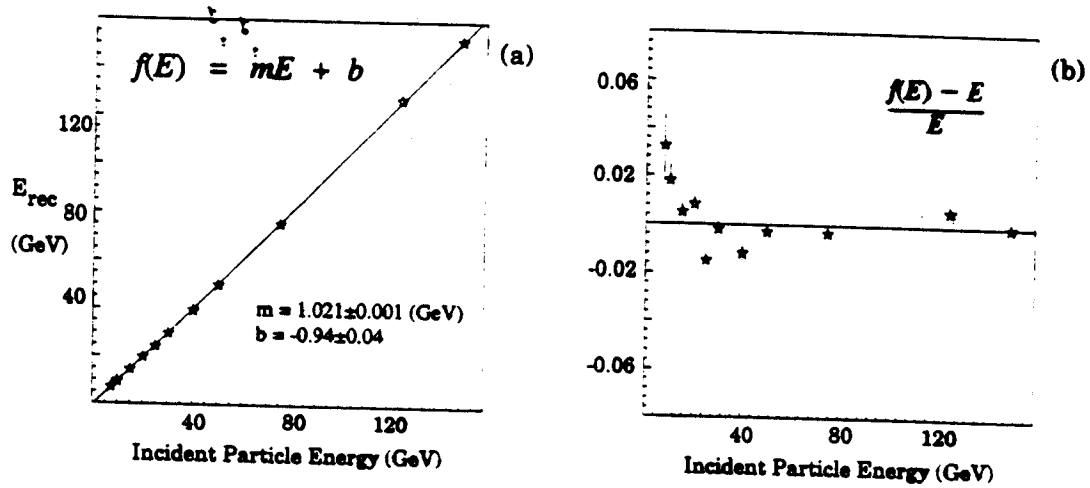

Figure 2 Reconstructed energies obtained using default weights at η=0.45

From the statistical errors given in Fig. 2(b), it is clear that the fit to a straight line is poor, and that there is a sizeable intercept. At this point, it is important to stress the fact that such a linear fit is of little use when optimizing jet resolution, since individual particle energies within a jet cannot be corrected through such a fit (because the individual energies cannot be unfolded from the total jet energy). Nonlinearities of the detector can be characterized, however, by the fractional difference between the reconstructed and incident energy, as shown in Fig. 3. The dashed curve corresponds to the previous linear fit to the data.

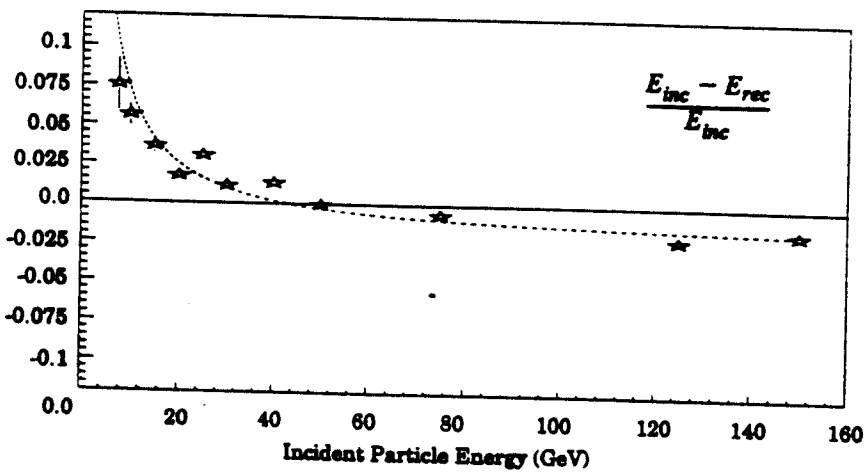

Figure 3 Fractional difference between incident and reconstructed energy using default weights at η=0.45

tion consists of the two high-energy sets, one set taken at η=0.05, and one at η=0.45, both at ϕ=31.6

The results from the various optimizations will be presented solely for gauging the effect of the various restrictions on single-hadron response. For application in DØ, all restrictions must be imposed upon any final set of weights, therefore only the results of the optimization using Set 6 will be compared to the default set to decide which of the sampling factors would be best for the DØ detector. However, in Chapter 6 we will be investigating ways to reduce the impact any of the restrictions through alternate implementations, so it is useful to study the relative magnitudes of the effects that the different constraints have on the energy resolution of individual hadrons.

Table 2 Definitions of sets of hadronic weights

Set	η Value	EM Weights	Energy Points
1	0.05	allowed to vary	individual
2	0.45	allowed to vary	individual
3	0.05	allowed to vary	simultaneous
4	0.45	allowed to vary	simultaneous
5	0.05,0.45	allowed to vary	simultaneous
6	0.05,0.45	fix at default	simultaneous

4.1 Results of Hadronic Optimizations

The sampling factors found for Sets 1 and 2 for each available energy are presented in Tables 3 and 4, respectively. As stated earlier, correlations between layers make any uncertainties cited on purely the sampling factors difficult to interpret. Therefore, no uncertainties are given. Instead, the resolution of the reconstructed energies will be used to provide an indication of the quality of the results.

default values. The hadronic weights are virtually the same for all optimizations.

Table 5 Sampling Factors for Sets 3, 4, 5, and 6

Set	EM1	EM2	EM3	EM4	FH1	FH2	FH3	CH
3	2.24	1.63	0.87	1.16	0.94	0.93	1.00	0.90
4	2.11	1.13	0.96	1.15	0.94	0.93	1.01	0.91
5	2.16	1.34	0.92	1.15	0.94	0.94	1.01	0.91
6	1.00	1.00	1.00	1.00	0.98	0.94	1.01	0.91

Tables 6 and 7 provide the parameters characterizing the optimizations for the data sets at η=0.05 and η=0.45, respectively. Although the character of the results for Sets 1 through 5 are not grossly different, Sets 1 and 2, which allow an energy dependence, provide the best results overall. The results using Set 6 show a larger degradation in resolution and linearity than the other sets, indicating that restricting the EM weights to those that are best for electrons has the biggest detrimental effect on the hadron response.

Table 6 Parameters from optimizations at η=0.05

	Fits to $\sigma(E)/E$		Fits to straight line	
Set	S (%)	C (%)	Slope	Intercept (GeV)
Default	51.1±1.0	3.56±0.21	1.022±0.001	-0.84±0.04
1	39.8±0.9	2.84±0.17	1.004±0.001	-0.51±0.03
3	42.7±0.9	2.45±0.21	0.999±0.001	-0.41±0.03
5	43.8±0.9	2.31±0.21	1.000±0.001	-0.49±0.03
6	47.2±0.9	3.30±0.20	0.995±0.001	-0.75±0.03

Table 7 Parameters from optimizations at η=0.45

	Fits to $\sigma(E)/E$		Fits to straight line	
Set	S (%)	C (%)	Slope	Intercept (GeV)
Default	48.0±0.9	3.87±0.16	1.021±0.001	-0.94±0.04
2	39.1±0.8	2.57±0.15	1.000±0.001	-0.21±0.03
4	40.2±0.8	2.38±0.17	1.001±0.001	-0.34±0.03
5	41.2±0.8	2.22±0.18	1.000±0.001	-0.30±0.03
6	45.9±0.9	3.51±0.16	0.994±0.001	-0.81±0.04

3 Optimization of Jet Resolution

All results in the following optimizations will be presented in terms of sampling factors, relative to the default weights. (The default weights correspond to dE/dx weights for the hadronic layers, and EM-layer weights chosen to optimize the response to electron).

Five different optimization schemes (OS) were implemented to try to improve the energy resolution of TB jets. OS-1 simply varies the relative scales between the EM and hadronic layers, and otherwise uses the default weights. OS-2 allows all weights to vary, and provides a single constant offset δ for the simultaneous optimization of all jet energies. OS-3 admits weights that depend on the reconstructed jet energy, and OS-4 allows weights that depend on the fraction of total reconstructed jet energy deposited in the electromagnetic layers (EM fraction). Finally, OS-5 implements a sequential optimization of energy-dependent and EM fraction-dependent variations. A summary of the various optimization schems is included in Table 1, and the details of the separate optimizations are given below.

Table 1 Summary of optimization schemes (OS)

OS	Parameters allowed to vary	# parameters	constant offset δ
1	scale factors describing relative contributions of EM and hadronic sections	2	set to zero
2	energy-independent weights describing the relative contributions of all layers	8	varies
3	parameters describing the energy-dependence of 8 layer weights	16	set to zero
4	parameters describing the EM fraction-dependence of 8 layers weights and a constant offset δ	18	varies
5	parameters describing the EM fraction-dependence and energy-dependence of 8 layer weights and a constant offset δ	8	varies for EM dependence set to zero for energy-dependence

3.1 Optimization of Relative Electromagnetic and Hadronic Scales (Scheme

Pg 2 of 79

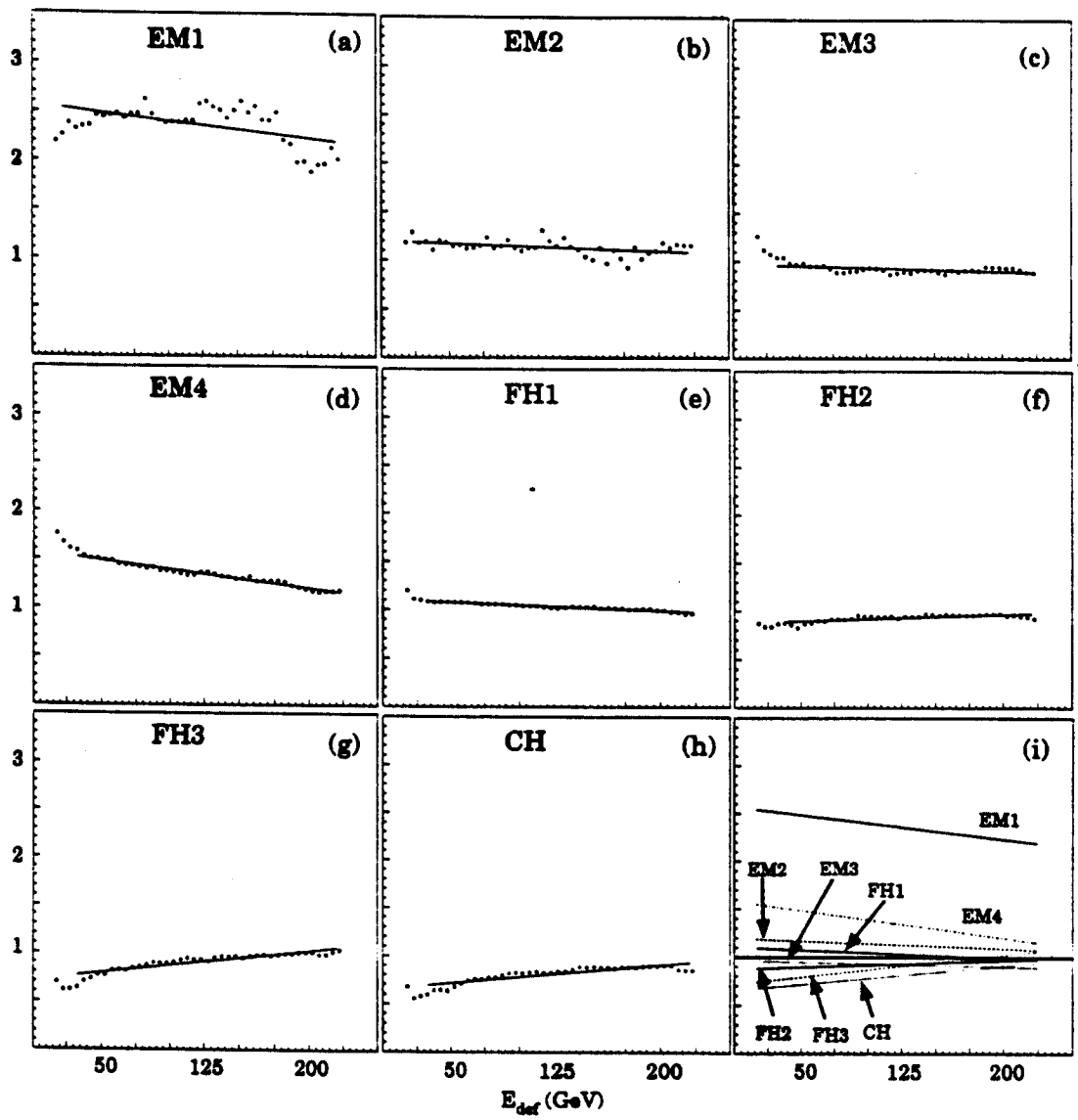

Figure 4 Sampling factors as a function of reconstructed energy (OS-3). The fits are to linear functions of the form $P_1 + P_2 E_{def}$ (see Table 4).

As can be seen in Fig. 4, the sampling factors at the extreme ranges of the energy scales do not seem to follow the trend observed in the center regions. By changing the ranges for the fits, we have determined that restricting the fits to the trend established by the central energy regions results in the best overall resolutions. The functions in the figures are plotted only over the energy ranges used in the fits.

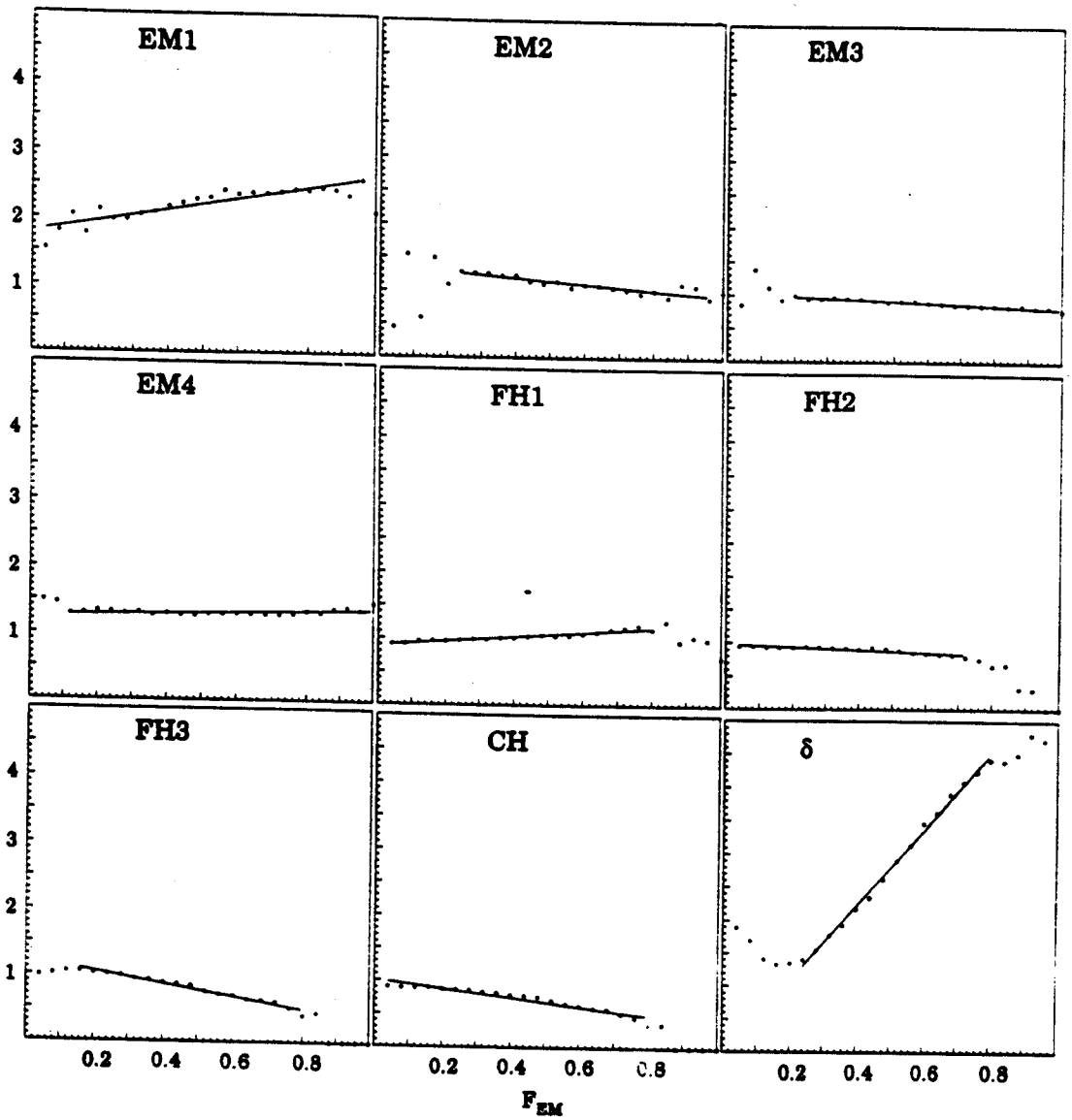

Figure 5 Sampling factors as a function of the fraction of the reconstructed energy in a TB jet that is deposited in the EM section. The fits are to linear functions of the form $P_1 + P_2 F_{EM}$ (see Table 5)

As seen in Fig. 5, the sampling factors for $F_{EM} \leq 0.2$ and $F_{EM} \geq 0.8$, (especially for δ) show marked deviations from the trend established in the rest of the range. This is caused primarily by the characteristic patterns of energy deposition for jets in these regions. For example, a jet with more than 90% of its energy in the electromagnetic section, will have little energy in CH that could be used to sharpen the CH sampling factor. Also, it should be

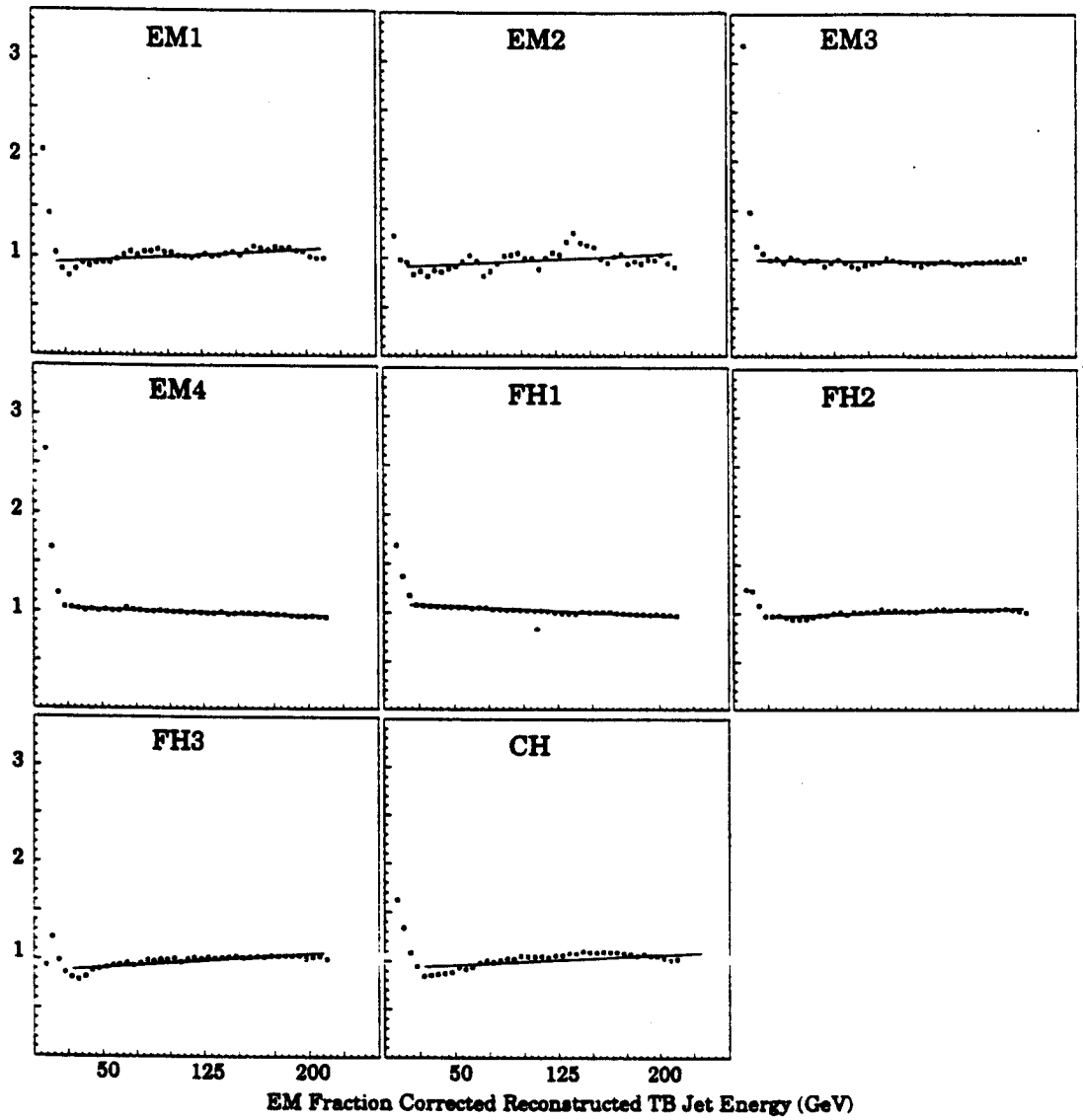

Figure 6 Sampling factors as a function of EM-fraction corrected reconstructed energy (OS-5). The fits are to linear functions of the form $P_1 + P_2 E_{rec}$ (see Table 6).

We also see in Fig. 6 that the sampling weights for the lowest energies show a marked difference from those for the higher energies. This indicates that using both EM fraction and energy-dependent corrections should have a negative impact on lowest-energy jets.

Df 2c79

3. These factors were then applied to the layer energies to find the optimized reconstructed energies E^i_{opt}, for any given optimization scheme i.
4. Finally, the corrections to the reconstructed TB jet energy, based on Table 7, were applied to determine the final energies E^i_{corr}.

These corrected and optimized energies were then compared with the parton energies to determine the jet resolution as a function of incident energy, as explained here. The reconstructed energies E^i_{corr} were separated into bands of 5 GeV. In parallel with the rescaling of energies of singles hadrons that was based on the measurements using PWCs, we also rescaled all the values of E^i_{corr} to the mean parton energy in the band. This eliminated any smearing in E^i_{corr} due to the spread in parton energies. We then calculated the standard deviation $\sigma(E)$ and mean $\mu(E)$ for each band of E^i_{corr} energies. The parameters of the resolution were then extracted by fitting Eq. (2) to the values of σ/μ. The parameters S and C from the fits, and their statistical uncertainties, are given in Table 8, and the corrected data for the various schemes with the fitted functions are shown in Fig. 8.

Table 8 Parameters describing resolution of reconstructed and corrected TB jet energies

OS-#	S (%/√E)	C (%)
Default	71.15±0.004	0.002±0.003
1	58.18±0.01	1.98±0.002
2	48.19±0.01	2.32±0.002
3	43.42±0.01	2.76±0.001
4	37.03±0.01	3.32±0.002
5	35.18±0.01	3.40±0.001

DØ 2674

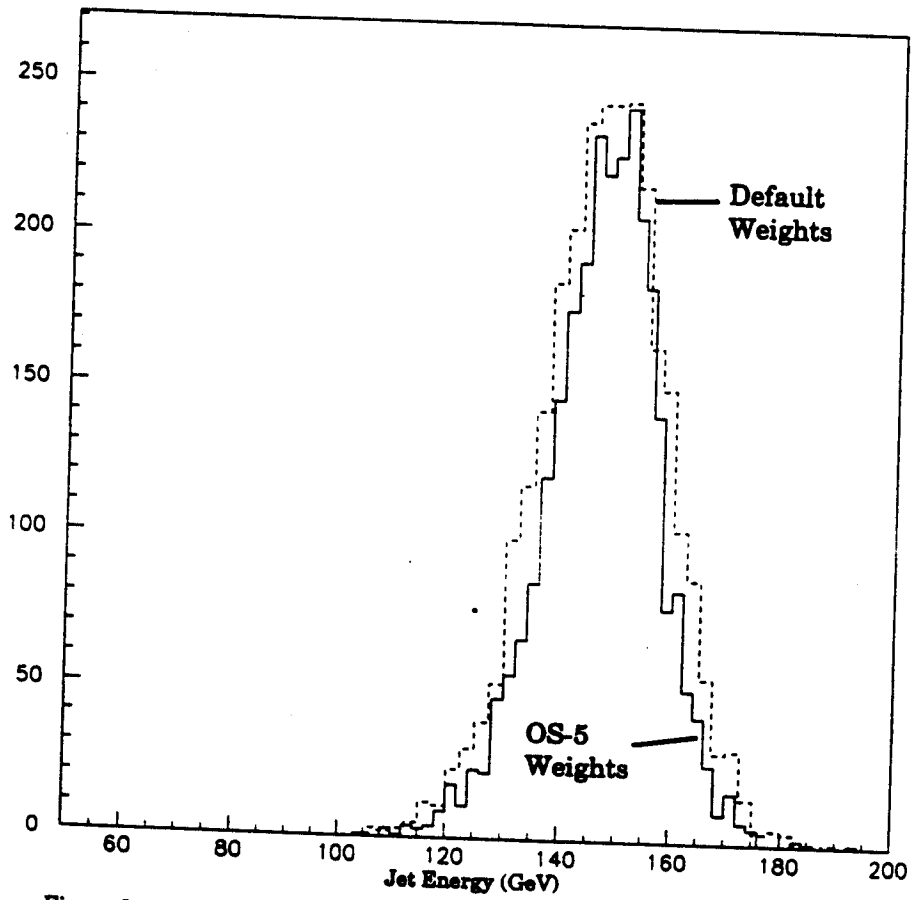

Figure 9 150 GeV Jet Response Distribution for Default Weights and OS-5 Weights

Because of the similarity of the plots in Fig. 8, and the fact that an increase in C can be compensated by a decrease in S in Table 8, if is difficult to gauge any improvement in jet energy resolution from the different optimization schemes. We therefore provide in Fig. 10 a comparison of the resolutions for the various schemes relative to the case using the default parameters.

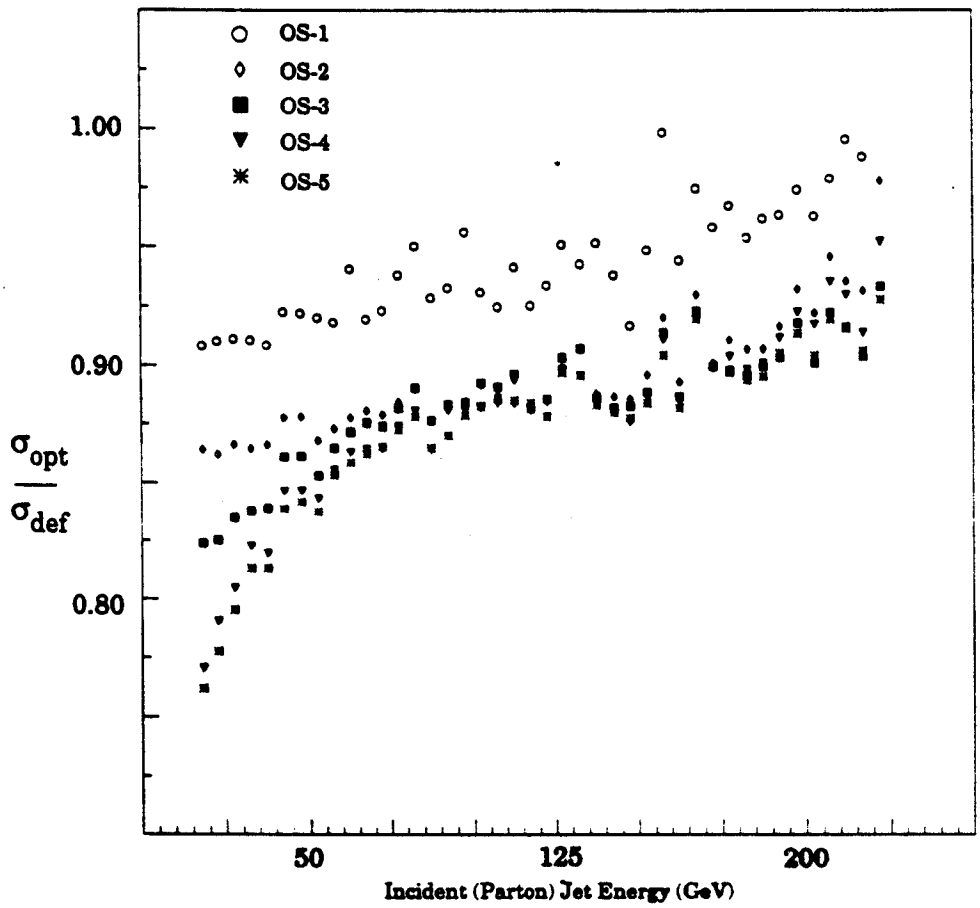

Figure 10 Ratio of optimized TB jet resolutions to the default values as a function of jet parton energy.

From Fig. 10, we see that while OS-1 improves the resolution over the default scheme, it is not as marked an improvement as those using the other schemes. The improvements for OS-2 to OS-5 are only slight at the highest energies, but more apparent at the lower energies. The OS-4 and OS-5 schemes appear to provide the best overall resolution.

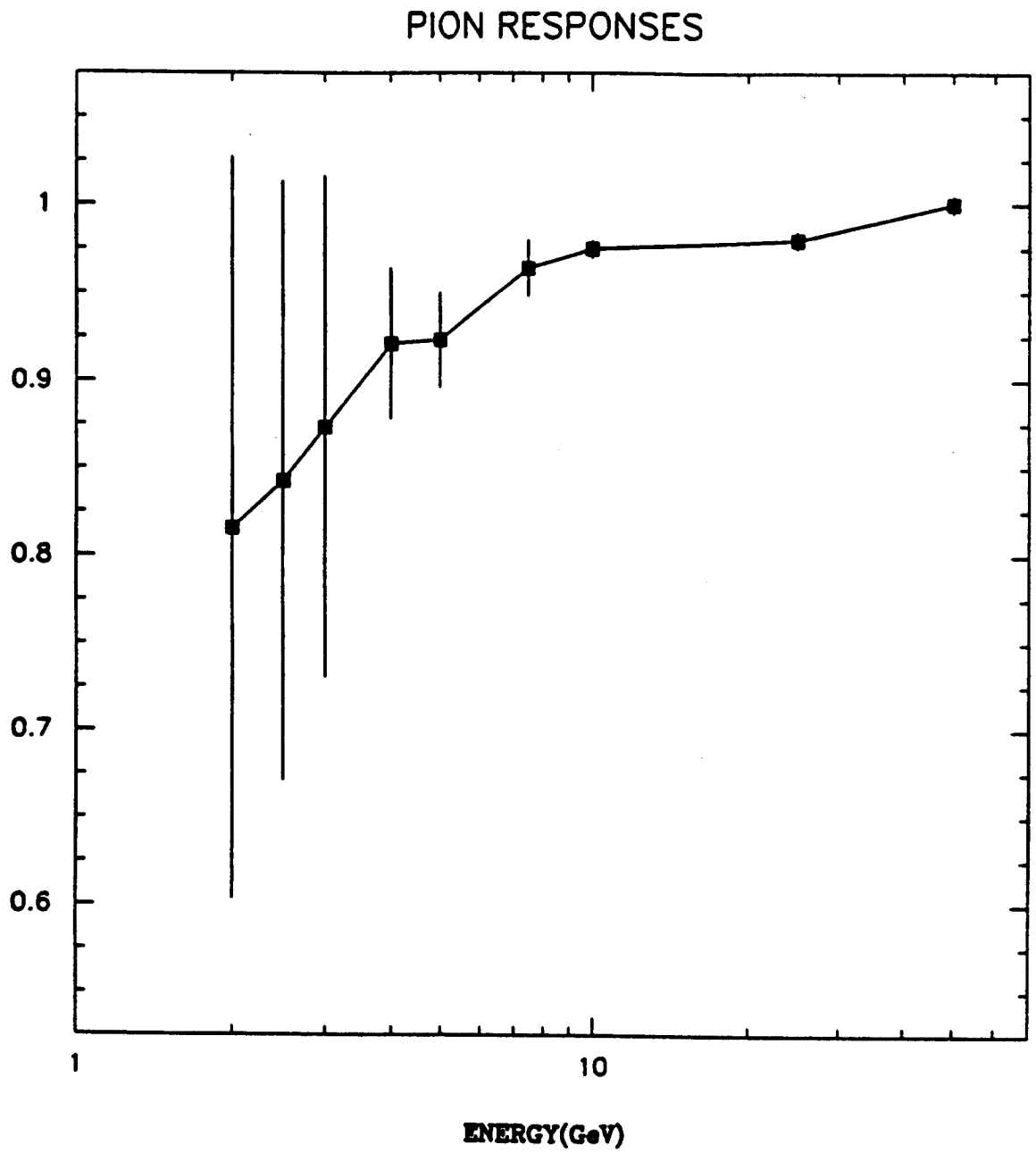

Figure 2: Test beam responses for pions.

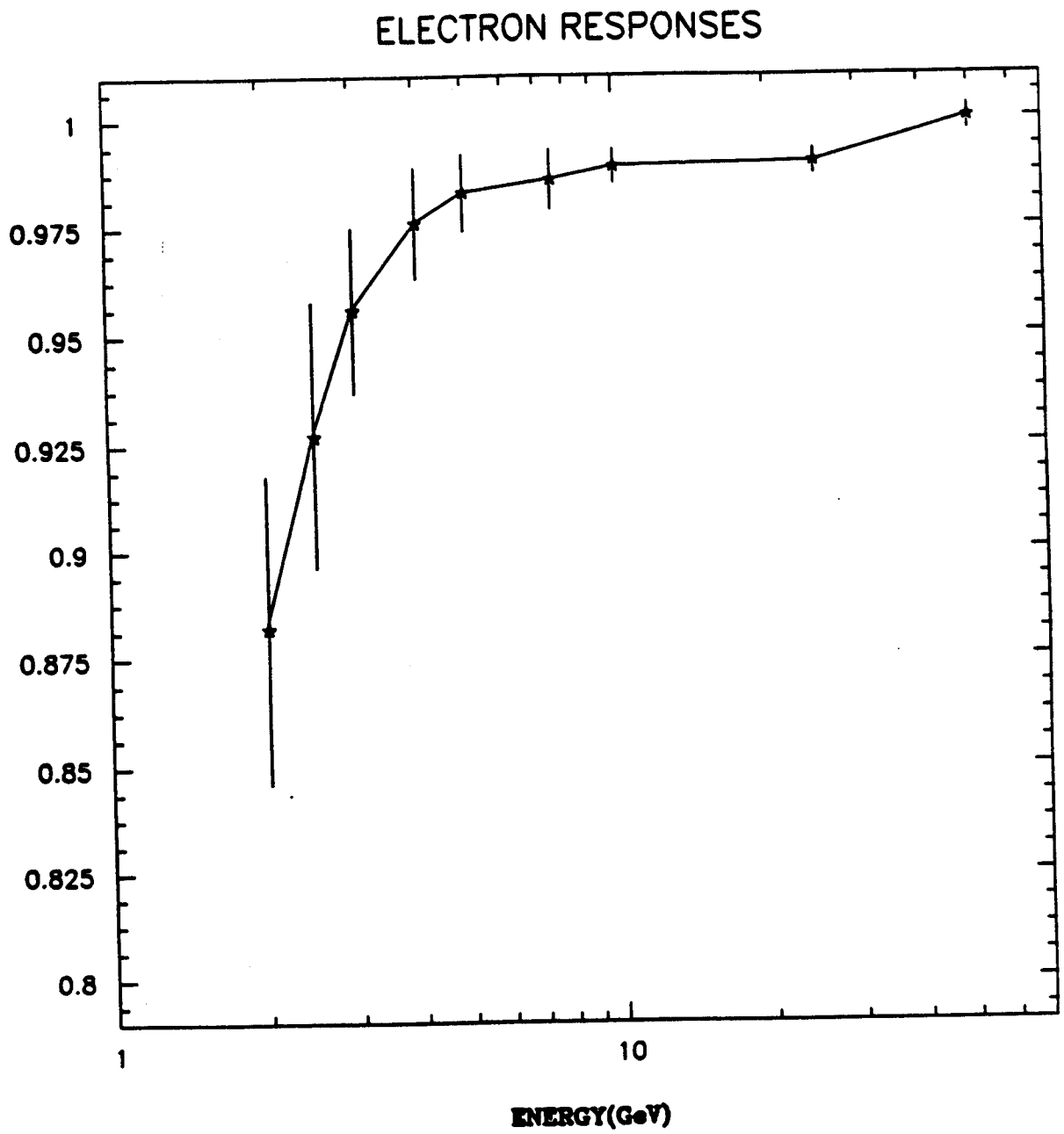

Figure 1: Test beam responses for electrons.

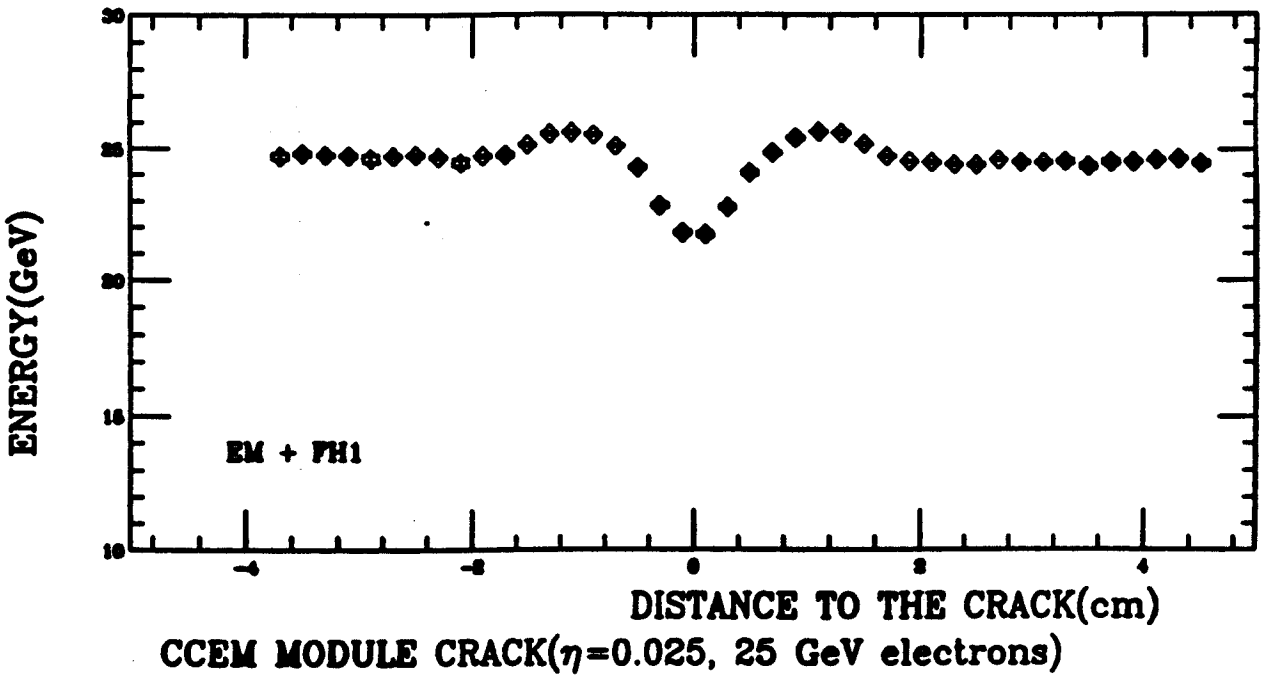

Figure 3: Response for 25 GeV electrons near a CCEM ϕ crack.

Figure 4[4]. Using this data to simulate the effects of the cracks on hadronic response results in about a 1% decrease in the jet response. Pions in the test beam were seen to be insensitive to CCEM cracks and likewise electron response was independent of CCFH crack position.

Event Generator Monte Carlo data

The jet simulation was accomplished using one of three event generators; Pythia, Herwig, or ISAJET. The Pythia jets do not include underlying event or initial state radiation while the Herwig and ISAJET results do. The use of three different event generators allows one to estimate the size of the errors

[4]Data from Welanthantri Dharmaratna.

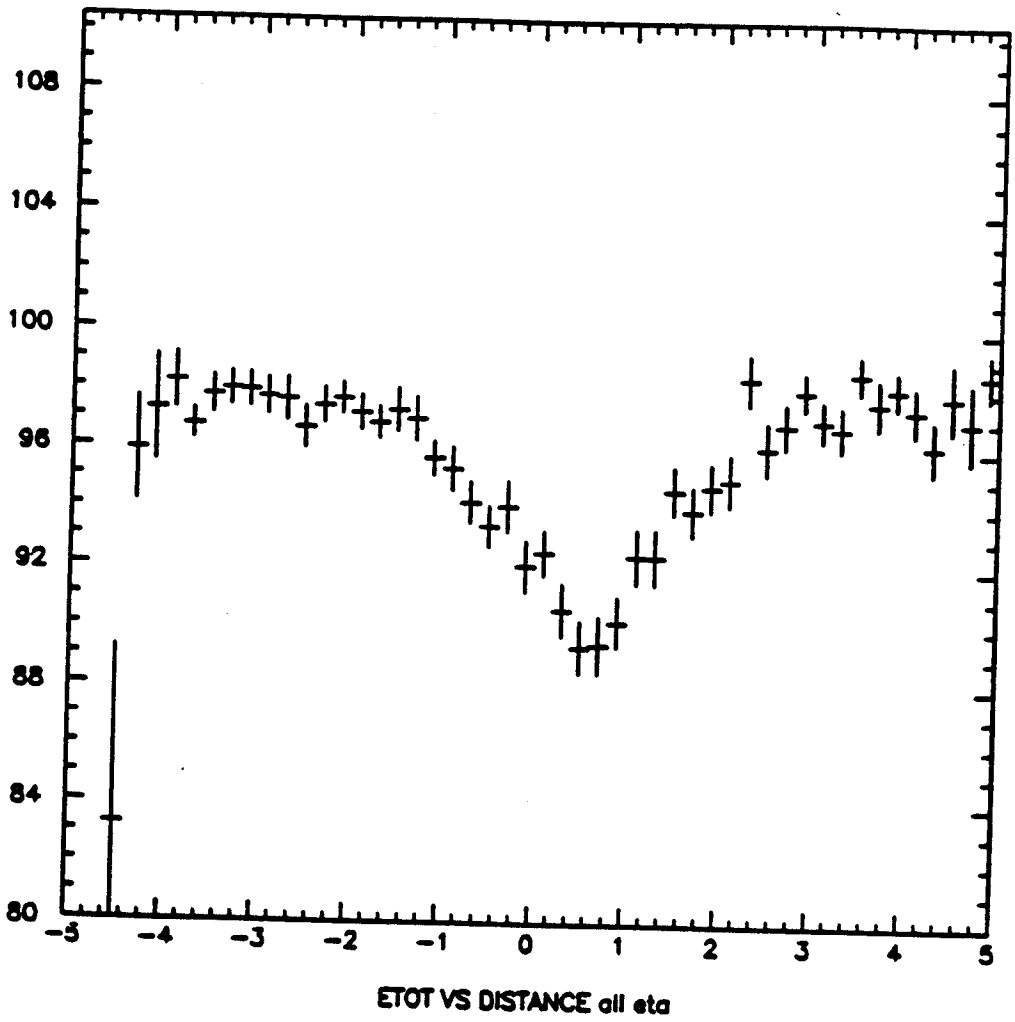

Figure 4: Response for 25 GeV pions near a CCFH ϕ crack.

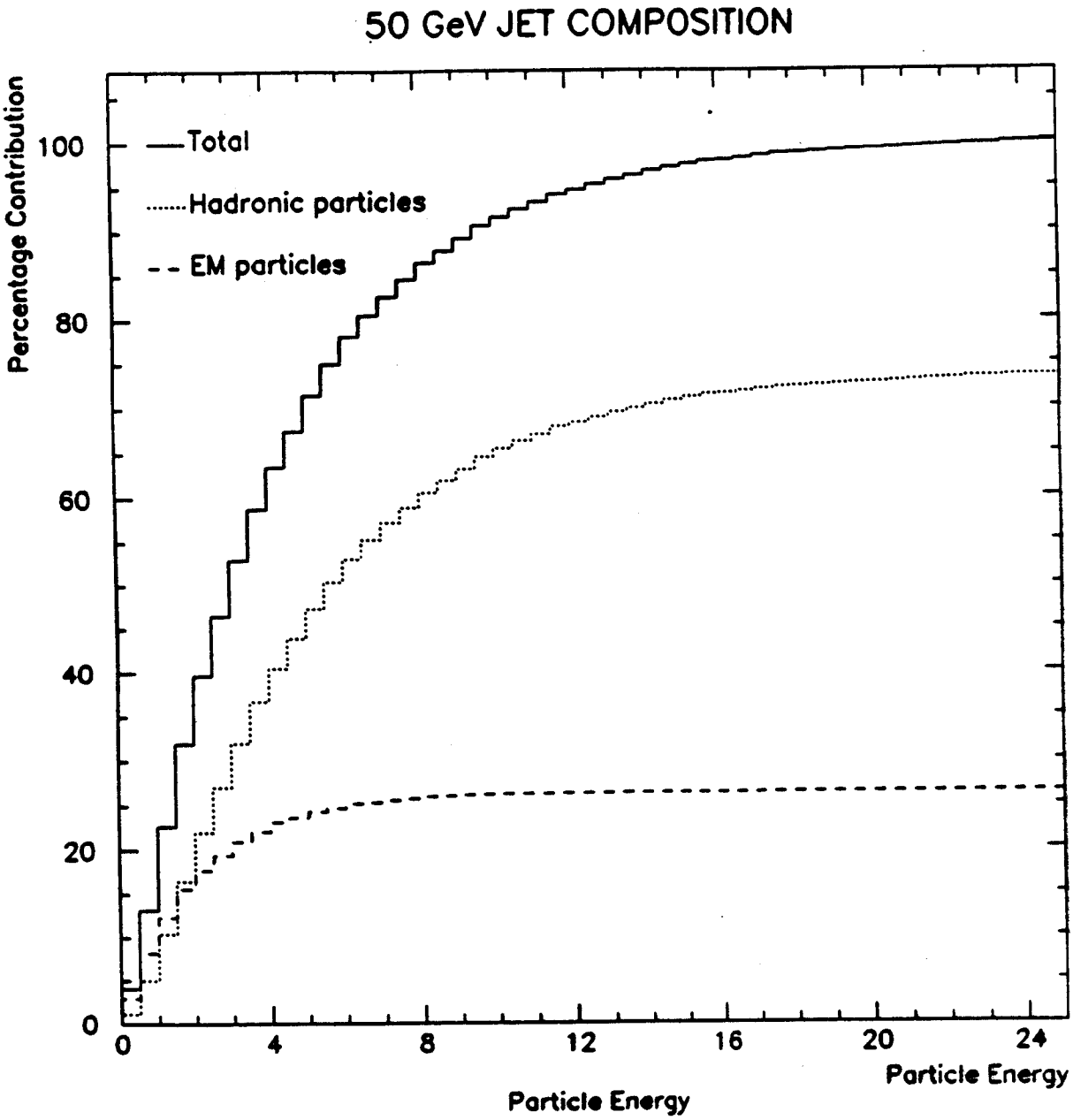

Figure 5: Particle composition of 50 GeV jets.

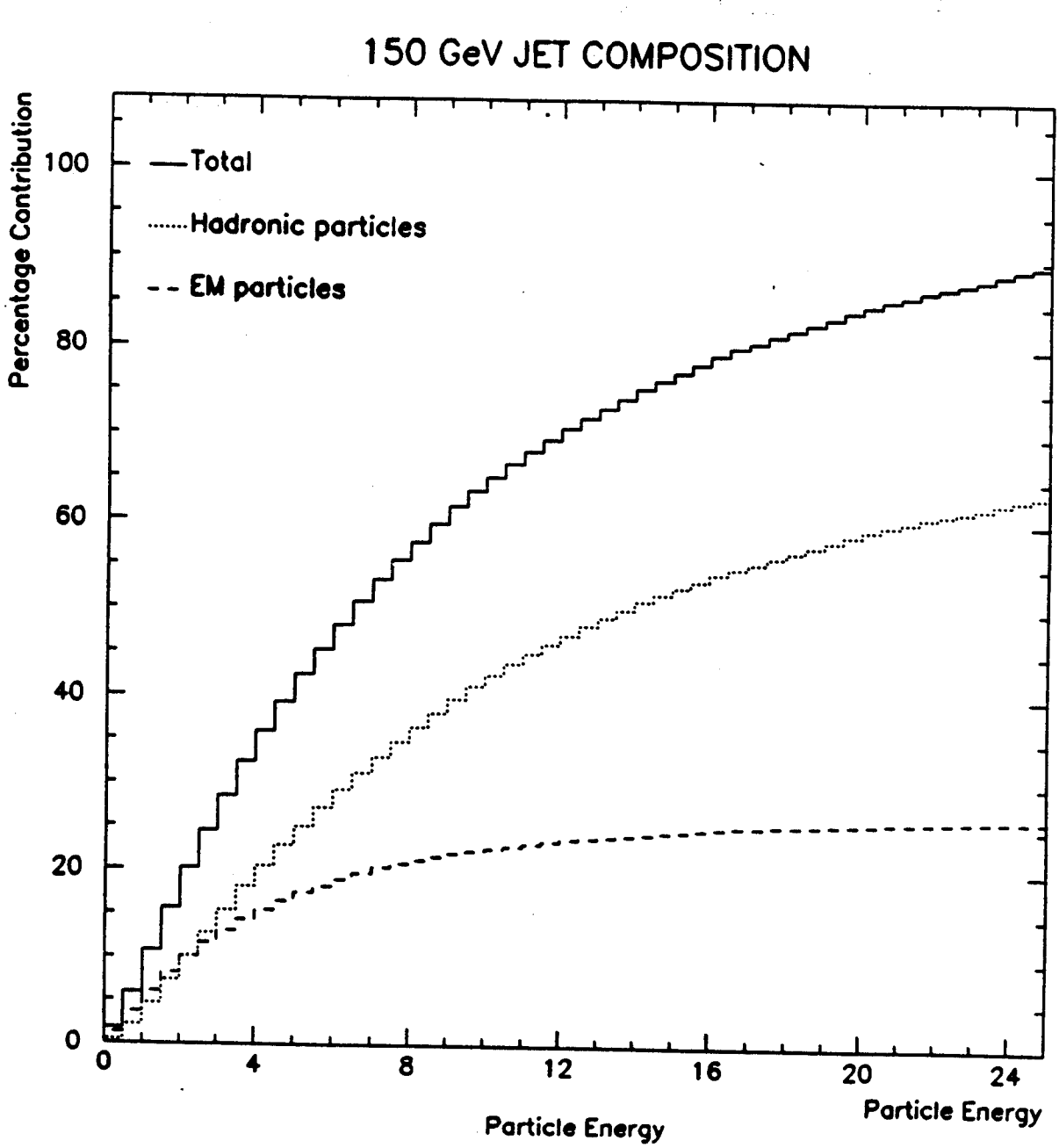

Figure 6: Particle composition of 150 GeV jets.

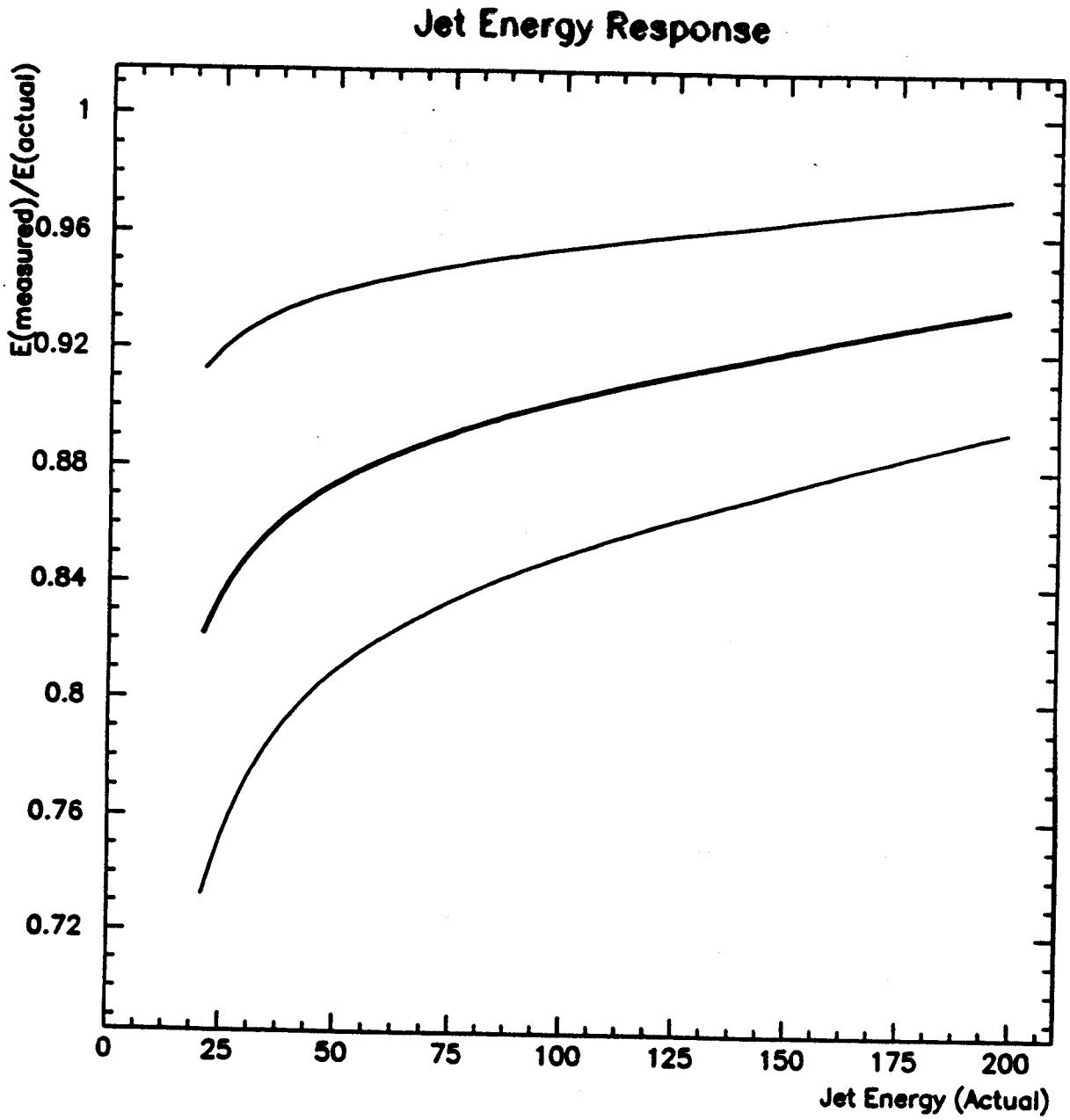

Figure 7: Nominal jet energy scale and limits of errors. The thick line is the nominal response and the thin lines are the upper and lower limits.